A Magnetohydrodynamic Model of Solar Wind Interaction with Asteroid Gaspra

Klaus Baumgärtel, Konrad Sauer, Alexander Bogdanov

The solar wind response to a small-sized magnetized body is modeled on the basis of a two-dimensional magnetohydrodynamic (MHD) plasma description including Hall current corrections (Hall-MHD model). Basic features of the magnetic signatures observed near Galileo's closest approach to asteroid Gaspra are reproduced, assuming Gaspra's magnetic dipole moment to be of the order of 10^{14} ampere·meters squared and tilted to the solar wind flow direction at an angle of about 45°.

On 29 October 1991, the Galileo spacecraft encountered the asteroid 951 Gaspra. Although the images of the small body attracted most interest, magnetic signatures near the closest approach have been reported and discussed by Kivelson *et al.* (*1*). Two large magnetic field rotations 1 min before and 2 min after its closest approach are the most important features seen in the magnetometer record. Although field rotations are common features of interplanetary magnetic perturbations, the authors suggest that the perturbations measured by the Galileo magnetometer in the solar wind are Gaspra-related, that is, produced by an intrinsic magnetic field of Gaspra. In support of this suggestion, we performed simulations on the solar wind interaction with a small-sized magnetized body in the framework of a two-dimensional (2D) MHD model. On the basis of these simulations, we argue that the magnetic moment of Gaspra was the source of the observed solar wind perturbation.

Methods of magnetohydrodynamics have been shown to account for the broad features as well as for many details of the solar wind interaction with large magnetized objects like the Earth (*2, 3*). In contrast, emphasis is here directed to a much weaker dipole, whose magnetic moment is orders of magnitude lower than that of the Earth. The question arises as to what extent the solar wind response to such an obstacle can still be described in terms of the traditional magnetospheric interaction (maintenance of a cavity from which the solar wind is excluded, a magnetosheath, and a bow shock). In a study on magnetic interaction of asteroids with the solar wind, Greenstadt (*4*) formulated three conditions to be met for a small magnetized body to form a mini-version of standard magnetospheric interaction. First, the field must be large enough at some distance above the body's surface to balance the solar wind ram pressure. Second, to rule out moon-like interaction, this distance must exceed the "stopping distance" of the solar wind, a distance of the scale of the electron inertia length c/ω_{pe}, which is of the order $(R_p R_e)^{1/2}$, where R_p and R_e denote the proton and electron gyroradius in the stopping field. Third, the lateral dimension of the asteroidal field should be at least commensurate with the proton gyroradius in the stopping field, otherwise edge effects come into play that preclude maintenance of a plasma-field interface. Combining these conditions, Greenstadt concluded that surface fields on the same order as that of the Earth's (5×10^4 nT) would be necessary for bodies of radii a few tens of kilometers to maintain magnetospheres. Since these required minimal levels of surface fields for minor bodies at 2 to 3.5 astronomical units (AU) distance from the sun are not unrealistic, magnetodynamic interaction of the solar wind with asteroids is plausible.

Max-Planck-Institut für extraterrestrische Physik, Außenstelle Berlin, 12489 Berlin, Germany.

For examination of solar wind interaction with an obstacle of "small" size, conventional MHD theory has to be modified by inclusion of Hall current effects. This accounts for the fact that in case of "small" characteristic spatial scales, protons are less strongly frozen to the magnetic field than electrons. Hall current effects cause dispersion of the relevant waves and introduce the ion skin length c/ω_{pi} and the ion gyration period $1/\Omega_i$ as natural length and time scales. This allows us to specify that a "small" body is understood as one having a size comparable to or smaller than the ion skin length. Gaspra orbits at a mean distance of 2 AU from the sun. The solar wind density at this distance is about one proton per cubic centimeter, resulting in an ion skin length of 230 km. Since the asteroidal magnetic field is expected to have a similar scale, Hall current modifications are required to be included for modeling of the solar wind interaction with Gaspra's magnetic moment in an MHD framework.

The observed magnetic field variations are mainly in the plane set up by the solar wind flow direction and the direction of the undisturbed upstream magnetic field, which was perpendicular to the flow direction during the encounter. This plane was chosen for our 2D simulation of the solar wind flow past a dipole (Fig. 1). The basic equations to solve cover the ion dynamics

$$\frac{\partial n_i}{\partial t} + \nabla \cdot (n_i \mathbf{v}_i) = 0 \tag{1}$$

$$\frac{\partial (n_i \mathbf{v}_i)}{\partial t} + \nabla \cdot (n_i \mathbf{v}_i \mathbf{v}_i) = \frac{e n_i}{m_i}(\mathbf{E} + \mathbf{v}_i \times \mathbf{B}) \tag{2}$$

the electron dynamics

$$\mathbf{E} = -\frac{1}{e n_e}\nabla p_e - (\mathbf{v}_e \times \mathbf{B}) \tag{3}$$

Ampere's law

$$\nabla \times (\mathbf{B} - \mathbf{B}_{\text{dipole}}) = \mu_o \mathbf{j} = \mu_o e(n_i \mathbf{v}_i - n_e \mathbf{v}_e) \tag{4}$$

Faraday's law

$$\frac{\partial \mathbf{B}}{\partial t} = -\nabla \times \mathbf{E} \tag{5}$$

and the condition of quasineutrality $n_e = n_i$. $\mathbf{B}_{\text{dipole}}$ denotes the vacuum field of the intrinsic magnetic moment of the body, $p_e = n_e k_B T_e$; other notations are standard. The ions are treated as a cold, weakly magnetized fluid; the electrons form an isothermal, strongly magnetized, massless continuum without resistivity. To solve these equations, we eliminate the electric field and apply the flux-corrected transport (FCT) scheme of Boris and Book (*5*) on a 128 by 128 mesh. At the right-hand (upstream) boundary the values of all variables are fixed to those of the inflowing solar wind, whereas free boundary conditions are adopted at the other boundaries. Initially, the simulation area is filled with undisturbed solar wind flow, and the vacuum dipole field is imposed impulsively at the start of the run. The simulation runs until a stationary state has been reached. This is generally the case after a time that the solar wind needs to cross the simulation box one to two times. The use of a 2D model forces the obstacle to degenerate to a line dipole. The field magnitude of a standard line dipole decreases with distance proportional to $1/r^2$. In order to maintain the stronger ($\sim 1/r^3$ in the far-field approximation) radial decrease of a 3D dipole field in our 2D simulation, we use a field derived from the vector potential

$$\mathbf{A} = \frac{\mu_0}{4\pi}\frac{\mathbf{p}_m \times \mathbf{r}}{r^3} \tag{6}$$

with $\mathbf{r} = (x, y, 0)$ according to

$$\mathbf{B}_{\text{dipole}} = \nabla \times \mathbf{A} = \frac{\mu_0}{4\pi}\left[\frac{3(\mathbf{p}_m \cdot \mathbf{r})\mathbf{r}}{r^5} - \frac{2\mathbf{p}_m}{r^3}\right] \tag{7}$$

Except for the factor 2 at the second term, this field is identical to a cut through a meridian plane of a 3D dipole with the dipole moment vector $\mathbf{p}_m$. The field actually used in the simulation is derived from a potential with $(r^2 + h^2)^{3/2}$ in the denominator instead of r^3. The smoothing parameter h removes the field singularity and controls the peak field strength at the origin, necessary for numerical reasons. It defines a near-zone around the dipole center in which an external magnetization current $\mathbf{j}_{ext} = \nabla \times \mathbf{B}_{dipole}$ in the z direction is present. This is the reason for keeping the term $\mathbf{B}_{dipole}$ in Ampere's law. In case of an ideal dipole, this term would vanish, except at the center.

The equally spaced 128 by 128 mesh cannot simultaneously resolve structures on the order of Gaspra's size (≈10 km) and cover the scale of the observations (some 1000 km). In order to provide a sufficient spatial resolution of the source region, however, the near-zone must cover at least several mesh points. This sets a limit for the choice of h and thus constrains the peak magnitude of the dipole field on the mesh.

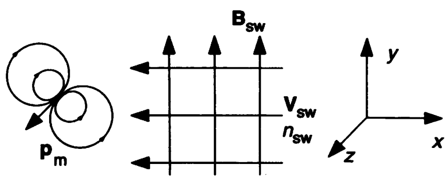

Fig. 1. Model of solar wind interaction with Gaspra's magnetic moment.

Parameters entering the model are on one side the strength of the dipole and its orientation in the xy plane and on the other side the solar wind flow Mach numbers $M_A = v_{sw}/v_A$ and $M_s = v_{sw}/c_s$, defined relative to the solar wind Alfven speed $v_A = B_{sw}/(\mu_0 m_i n_i)^{1/2}$ and to the ion acoustic velocity $c_s = (k_B T_{e,sw}/m_i)^{1/2}$, respectively. The solar wind velocity at 2 AU is about 300 km/s. This combines together with the measured interplanetary magnetic field (IMF) strength of 1.7 nT to give an Alfven Mach number $M_A = 8$. The solar wind plasma beta is assumed to be on the order of or less than 1, that is, $M_s \geq M_A$. The dipole-related parameters have been freely varied to reach a best fit to the observations. Figure 2 illustrates the steady-state response of the solar wind to a dipole of moment $p_m = 1.5 \times 10^{14}$ A·m², tilted to the solar wind flow direction by 45°. Note that the dipole field is cut to a peak value of less than twice the magnitude B_{sw} of the undisturbed IMF as a result of taking the smoothing parameter h to be four times the grid spacing. This is roughly an order of magnitude smaller than the field strength required to balance the solar wind ram pressure for $M_A = 8$. Although the dipole cannot stop the solar wind, a magnetosphere is formed around the small body, exhibiting a significant asymmetry relative to the Gaspra-sun line. It results apparently from the different directions of the opposing vacuum dipole field relative to the solar wind field in the "north" and the "south" hemisphere. The asteroidal field appears to leak into the solar wind field resulting in a stationary draping pattern as shown in the bottom panel of Fig. 2. Both proton density and magnetic field pile up near to the dipole center, but there is no stagnation point, as expected. A wake region is established downstream of the obstacle with a somewhat disturbed proton flow. It contains a curved current sheet that also separates regions of enhanced and depleted proton density. Field and flow return gradually to their upstream configuration within the wake. The response features resemble a Mach cone structure with strongly asymmetric wings. The large an-

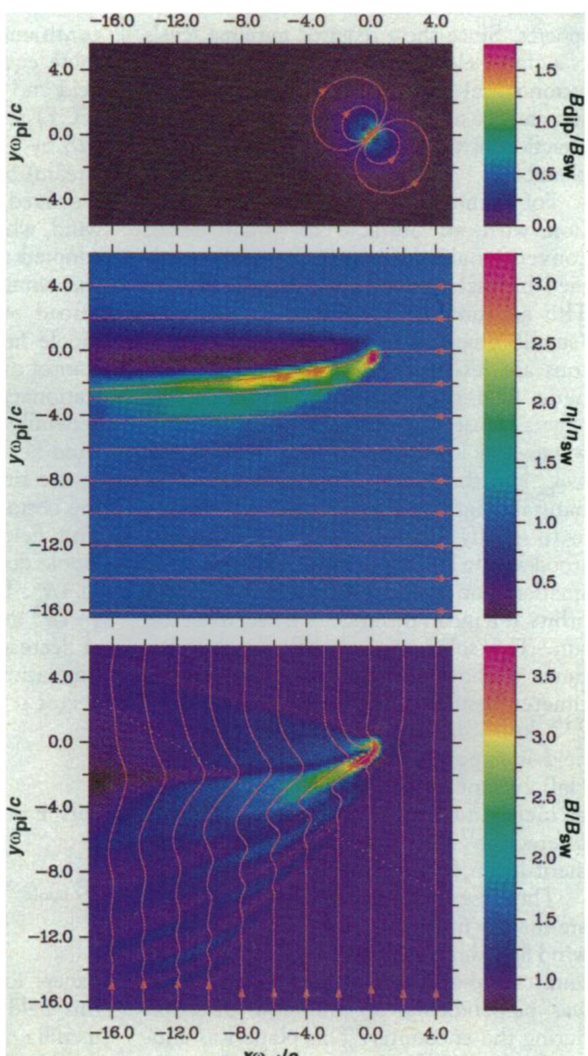

Fig. 2. Stationary response of the solar wind flow at 2 AU (Mach numbers $M_A = 8$, $M_s = 12$) to a small body with an intrinsic magnetic dipole of moment $\mathbf{p}_m = 1.5 \times 10^{14}$ A·m², tilted to the flow direction by 45°. Distances are scaled with the proton skin length $c/\omega_{pi} = 230$ km; proton density and magnetic field are normalized by their undisturbed upstream values ($n_{sw} = 1$ cm^{-3}, $\mathbf{B}_{sw} = 1.7$ nT, respectively). Mesh size, $\Delta = 0.16c/\omega_{pi} = 35$ km; dipole near-zone, $h = 0.7c/\omega_{pi} = 160$ km ≈ 4Δ. (**Top**) Vacuum dipole field. (**Middle**) Proton density and stream lines of the proton flow. (**Bottom**) Magnetic field magnitude and magnetic field lines. The dotted line is the projection of the Galileo spacecraft trajectory onto the simulation plane.

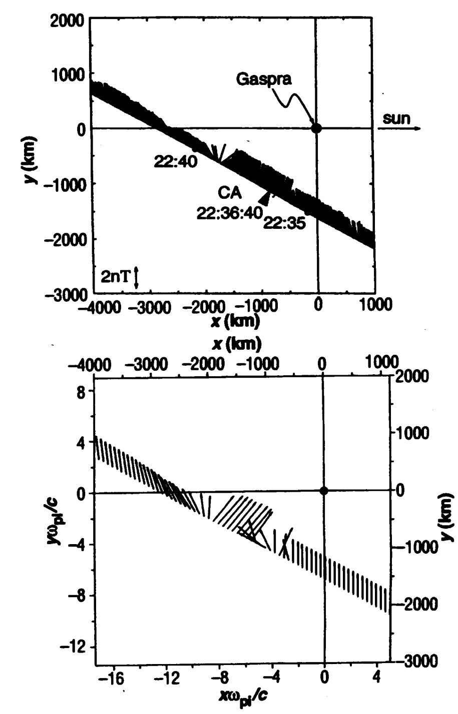

Fig. 3. Comparison of the observed (**top**) [reproduced from (*1*)] and the calculated (**bottom**) variation of the magnetic field vector along the projection of the Galileo trajectory onto the simulation plane. Closest approach (CA) is given in universal time. Gaspra is not drawn to scale.

gle (≈45°) from the body at which the field perturbation is first seen is much larger than the opening angle of a Mach cone associated with the fast MHD mode for $M_s \geq M_A = 8$. This indicates the excitation of dispersive Hall-MHD modes with large group velocities (whistler-type waves). We suggest that the stripes seen in the magnetic field plot of Fig. 2 are the result of coherent interaction of such waves with wavelengths comparable to the spatial scale of the obstacle, moving away from the source region and swept back by the solar wind flow. The stripes are not seen when Hall current corrections are suppressed in the simulation. In Fig. 3, the observed and calculated variation of the magnetic field vector along the Galileo trajectory are compared. The spacecraft motion is from right to left. As seen from this plot, the model reproduces the observed field variation fairly well, in particular the two field rotations. The first rotation indicates that the spacecraft passes from the undisturbed solar wind into the region dominated both by Gaspra's deformed intrinsic field and whistler wave activity. The second rotation is associated with the current-sheet crossing. Figure 4 comprises the model predictions with respect to plasma variations along the spacecraft trajectory (proton density and proton velocity). Changing the peak magnitude of the dipole field by variation of the smoothing parameter h (within the range limited by the onset of numerical instability) does not seriously affect the results. This indicates that the particular field structure near the origin is not crucial in determining the general features of the response.

The results suggest that the solar wind interaction with Gaspra's magnetic moment produces a physical situation of intermediate character in the sense that it may be placed between the classical Mach cone type response, characteristic for point-like obstacles, and the standard magnetospheric model for large magnetized objects.

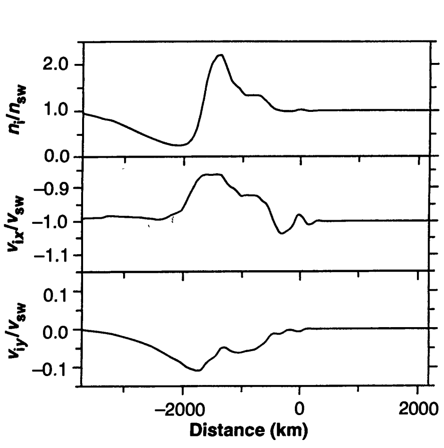

Fig. 4. Variation of proton density and velocity along the spacecraft trajectory as predicted by the simulation. Spacecraft motion from right to left, closest approach marked by zero.

The model imposes several limitations (2D instead of 3D, non-ideal line dipole with limited peak field strength, cold ions, artificial resistivity introduced by the numerical code working on a discrete mesh) that could make our results of limited interest. The most serious of them seems to be the cut of the dipole field magnitude, required for numerical reasons. However, the fact that most of the typical features of the observations are reproduced by the simulations encourages us to believe that the model covers the basic mechanism of the interaction, and may prepare the way for 3D Hall-MHD calculations.

In summary, our results indicate that the observed magnetic field variations near Gaspra can be understood as the result of the solar wind interaction with an intrinsic magnetic moment of Gaspra of the order of 10^{14} A·m^2, tilted to the solar wind flow direction by an angle of about 45°.

REFERENCES AND NOTES

1. M. G. Kivelson *et al.*, *Science* **261**, 331 (1993).
2. J. R. Spreiter and A. Y. Alksne, *Ann. Rev. Fluid Mech.* **2**, 313 (1970).
3. R. J. Walker, T. Ogino, M. Ashour-Abdalla, in *Solar System Plasma Physics*, J. H. White Jr, J. L. Burch, R. L. Moore, Eds. (*Geophysical Monograph 54*, American Geophysical Union, Washington, DC, 1989).
4. E. W. Greenstadt, *Icarus* **14**, 374 (1971); in *Physical Studies of Minor Planets*, T. Gehrels, Ed. (NASA Sp.-267) (1971), p. 567.
5. D. L. Book, J. P. Boris, and S. T. Zalesak, in *Finite-Difference Techniques for Vectorized Fluid Dynamics Calculations*, D. L. Book, Ed. (Springer-Verlag, New York, 1981), pp. 29–41.

6. We are grateful to M. Kivelson and D. Southwood for providing a preview on the magnetometer data and for pointing us to the two papers of E. W. Greenstadt and to G. Haerendel for helpful comments.

12 August 1993; accepted 22 November 1993

Electric Field–Induced Concentration Gradients in Lipid Monolayers

Ka Yee C. Lee, Jürgen F. Klingler, Harden M. McConnell

Externally applied electric field gradients gave rise to lateral concentration gradients in monolayers of certain binary lipid mixtures. For binary mixtures of dihydrocholesterol and dimyristoylphosphatidylcholine, the application of an electric field gradient at pressures below the critical pressure produced a liquid-liquid phase separation in a monolayer that is otherwise homogenous. At pressures slightly above the critical pressure, a field gradient produced a large concentration gradient without phase separation. The lipid concentration gradients can be described by equilibrium thermodynamic chemical potentials. The observed effects appear to be relevant to the structure and composition of biological membranes.

Epifluorescence microscopy has been used to observe coexisting two-dimensional liquid phases in binary mixtures of phospholipids and steroids at the air-water interface (*1–7*). Monolayer studies of binary mixtures of phosphatidylcholines and cholesterol were initially stimulated by evidence for coexisting liquid phases in bilayers composed of these lipids and by the possibility that such coexisting phases might be significant for the structure and function of biological membranes (*8*). We devised a technique that uses an inhomogeneous electric field to manipulate lipid monolayer domains (*9, 10*). Modest electrical potentials gave rise to substantial lateral concentration gradients in lipid monolayers with compositions and properties that potentially mimic some biological membranes. The electrical field strengths were comparable with those present in biological membranes (~10^7 V/m).

We studied a binary mixture of dihydrocholesterol (DChol) and dimyristoylphosphatidylcholine (DMPC). This mixture forms two immiscible liquid phases at certain temperatures and surface pressures π and exhibits a mixing-demixing critical point (Fig. 1) (*11*). At a critical composition of $x_1 = 0.3$ (x_1 is the mole fraction of DChol), the two liquid phases, one rich in DChol and the other rich in DMPC, merge into a single phase of uniform composition at the critical point upon increase in lateral pressure or temperature (*8*). Domain sizes and shapes in the liquid-liquid coexistence region depend on competition between line tension at the domain boundary and dipole-dipole electrostatic repulsion between molecules within and between the domains (*2*).

Because of the dipole moment difference between DChol and DMPC molecules, an electric field gradient induces preferential

Department of Chemistry, Stanford University, Stanford, CA 94305–5080.